Supplementary Information for:

A comprehensive study of the macro- and mesopores size distributions in polymer monoliths using liquid chromatography and complementary physical characterization techniques

Sam Wouters[1], Tom Hauffman[2], Marjo C. Mittelmeijer-Hazeleger[3], Gadi Rotherberg[3], Gert Desmet[1], Gino V. Baron[1], Sebastiaan Eeltink[1*]

[1]Vrije Universiteit Brussel, Department of Chemical Engineering, Pleinlaan 2, B-1050 Brussels, Belgium

[2]Vrije Universiteit Brussel, Department of Materials and Chemistry, Research group of Electrochemical and Surface Engineering, Pleinlaan 2, B-1050 Brussels, Belgium

[3]University of Amsterdam, Van 't Hoff Institute for Molecular Sciences, Science Park 904, 1098 XH Amsterdam, The Netherlands

(*) corresponding author

Pleinlaan 2, B-1050, Brussels, Belgium

Tel.: +32 (0)2 629 3324, Fax: +32 (0)2 629 3248, E-mail: seeltink@vub.ac.be

1 Materials and Methods

2-acrylamido-2-methylpropane sulfonic acid (AMPS, 99%), 1,4-butanediol (99%), butylmethacrylate (BMA, 99%), ethyldimethacrylate (EDMA, 98%), and 1-propanol (99.9%) were purchased from Sigma Aldrich (Bornem, Belgium). BMA was purified over activated alumina to remove inhibitor, all other products were used as received. 5.0 µm Hypersil particles (120 Å, C_{18} functionality) was obtained from Agilent Technologies (Waldbronn, Germany).

Table S1 list the compositions of the polymerization mixtures used in this study to synthesize acrylate monoliths.

Table S1. Polymerization mixture compositions in wt% for AMPS functionalized poly(butylmethacrylate-*co*-ethyldimethacrylate) monoliths.

BMA	EDMA	1,4-butanediol	1-propanol	$AMPS_{(aq)}$	AIBN
24.0	16.0	18.0	37.0	5.0**	3.0*
24.0	16.0	20.0	35.0	5.0**	3.0*

* Percentage of AIBN initiator relatively to mass of monomers. ** 1/6 wt% AMPS in water to yield 2.4 wt% of AMPS relative to monomer weight.

2 Results and discussion

Physical characterization experiments such as mercury-intrusion porosimetry (MIP) and argon or nitrogen adsorption desorption require a sufficient sample mass. To verify the validity of using data obtained from bulk samples (prepared in 2 mL sample vials) to complement data obtained directly on monoliths synthesized in capillary columns format (200 µm i.d.), the morphology was compared using SEM. Fig. S1 provides this comparison for a styrene-based monolith prepared with 14.0 wt% THF in bulk and in capillary. The larger format employed appears to have a limited effect on the domain size.

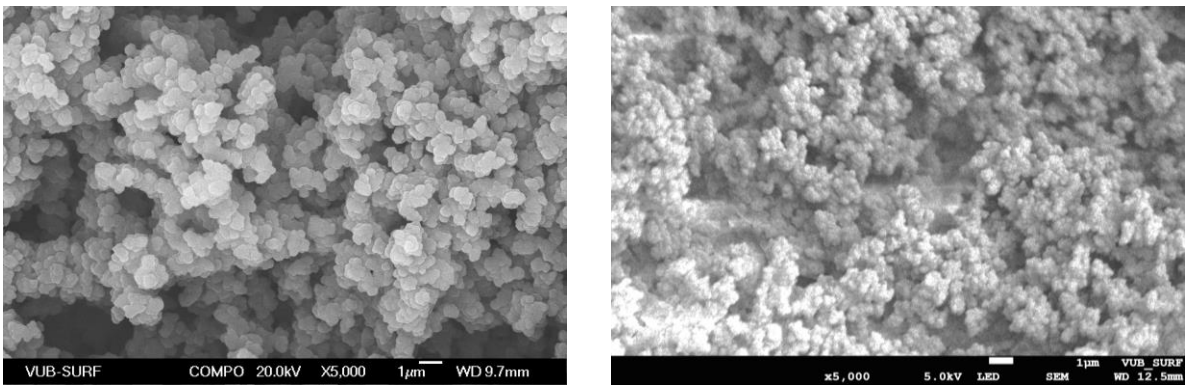

Figure S1. Scanning electron micrographs of P(S-*co*-DVB) monoliths synthesized with 14.0 wt% THF 200 µm i.d. capillary tubing (left) and in a bulk format (right).

The monolithic materials were studied with MIP and a commonly used representation plots log differential pore volume, D_3 or *dV/dlogD* on a logarithmic abscissa (Fig. S2). This is a useful representation method considering the fact that pore sizes of several order of magnitude are scanned in one measurement.

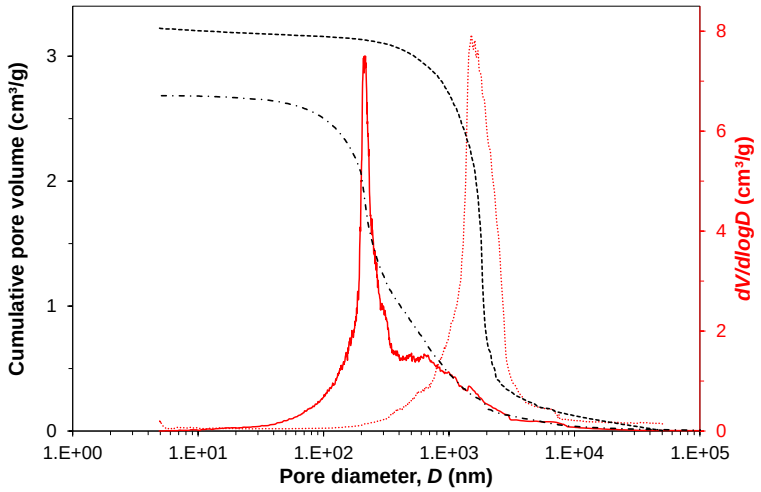

Figure S2. Mercury-intrusion porosimetry data for bulk samples of poly(S-*co*-DVB) monoliths synthesized with 14 wt% and 17.5 wt% of THF. The cumulative pore volume D_0 and pore size distribution D_3 are plotted as a function of pore diameter on a log scale. D_0 14.0 wt% THF (dashed line), D_0 17.5 wt% THF (dash-dotted line), D_3 14.0 wt% THF (dotted line), D_3 17.5 wt% (solid line).

To compare the width of pore-size distributions observed for the polymer monolithic stationary phases, MIP was performed on a typical particulate stationary phase. The 5 µm particles were introduced in the sample holder. Results are shown in Fig. S3. A relatively broad PSD is also observed here. The signal increase around 12 nm is caused by the fully-porous nature of these particles, containing 120Å mesopores.

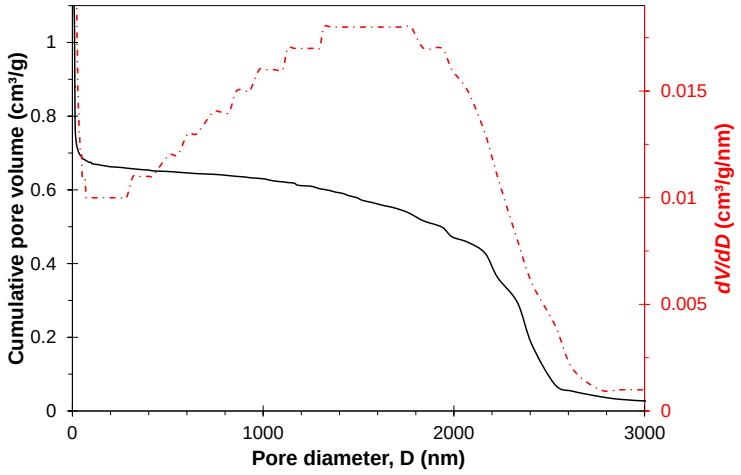

Figure S3. Mercury-intrusion porosimetry data for 5 µm particles removed from a conventional column. Pore diameter is plotted on a linear scale as a function of the cumulative pore volume D_0 (solid line) and pore size distribution D_2 (dashed-dotted line).

Adsorption-desorption experiments were also performed using the poly(styrene-*co*-divinlybenzene) monolithic matrix using nitrogen as an adsorbate, shown in Fig. S4. In comparison with results obtained using Ar, the hysteresis is smaller, *i.e.*, less swelling is taking place, which is in agreement with its larger size and increased matrix rigidity given the lower temperature used in such experiment.

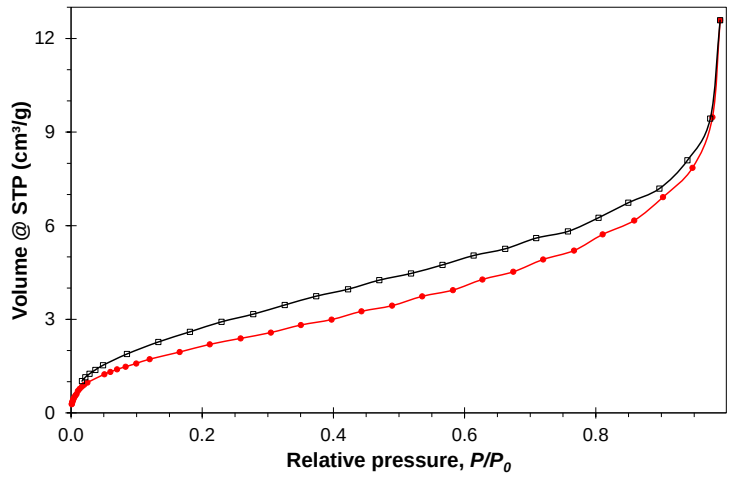

Figure S4. Nitrogen adsorption (○) and desorption isotherms (□) for a bulk P(S-*co*-DVB) monolith synthesized with 17.5 wt% of THF.

A test was also conducted where longer waiting times were used for each data point collected, which resulted in small increase in adsorption-desorption hysteresis, although the total adsorbed amount was not found to be significant larger.

To further study the swelling behavior for the styrene-based monoliths, a scanning experiment was performed (with nitrogen), as shown in Fig. S5. In a series of adsorption-desorption experiments, the scanned range of relative pressures was reduced. The adsorption behavior is coinciding for all experiments, and desorption hysteresis is becoming smaller with the reduction of the scanned range, indicating that gas is penetrating the polymer over the entire range of relative pressures during adsorption and not only at a very high relative pressure (if the latter would be the case, there would be no adsorption-desorption hysteresis when scanning to, *e.g.*, P/P_0 = 0.5). It is possible that with increasing relative pressures, gas is pushed inside increasingly small cavities, rather than the usual adsorption mechanism in gas adsorption where small pores fill first.

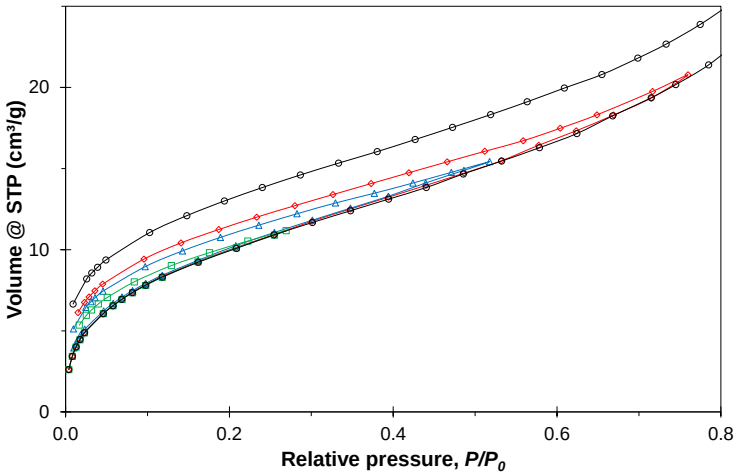

Figure S5. Nitrogen adsorption and desorption isotherms (zoom in, abscissa limited to P/P_0 = 0.8) for a bulk P(S-*co*-DVB) monolith synthesized with 17.5 wt% of THF. Adsorption was limited conducted over the full range of relative pressures, until complete condensation (○) and to P/P_0 of approximately 0.75 (◊), 0.55 (△) and 0.25 (□).

To study possible parallels of our findings for styrene-based monoliths with different classes of monoliths employing different monomer-porogen systems, two acrylate monoliths were synthesized featuring different porous properties. AMPS was incorporated in the backbone to create ion-exchange functionalities useful for our future research. Fig. S6 shows SEM micrographs obtained for the monoliths synthesized with compositions listed in Table S1, and Fig. S7 shows the corresponding pore-size distributions obtained via MIP. Similar to the styrene system, the variation in good-to-bad-solvent

ratio yields a material with a smaller domain size. The differences in average pore size (approximately 200 nm and 1 µm) are smaller for the two acrylates when compared to the styrenes, which is in agreement with the smaller difference in domain sizes (approximately increasing from 150 nm to 300 nm) as observed in the SEM micrographs for the acrylates. Also note that the monolith with smaller feature size has a smaller cumulative pore volume within the studied range compared to the monolith with a larger feature size, as also observed for the styrene-based monolithic materials.

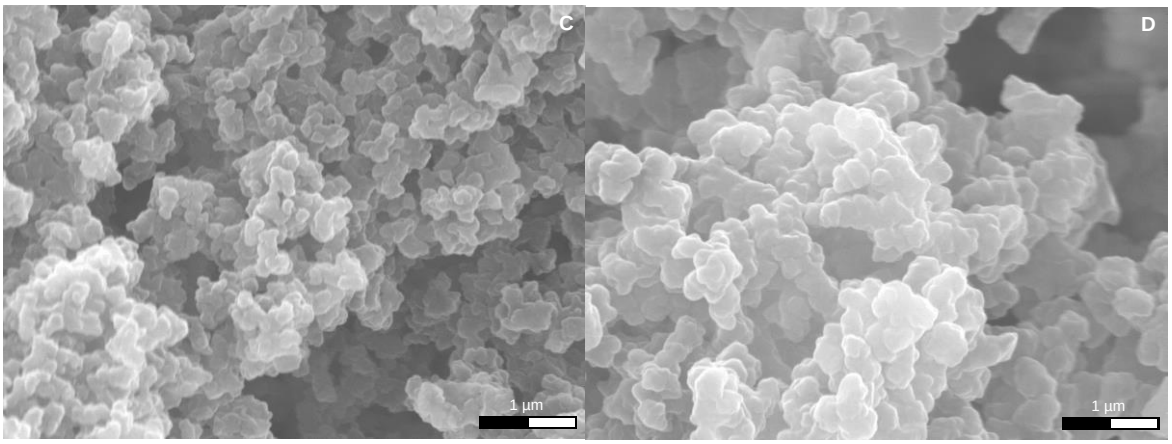

Figure S6. Scanning electron micrographs of the cross-sections of fused-silica capillary monolithic columns obtained via secondary electron imaging of P(BMA-*co*-EDMA-*co*-AMPS) monoliths synthesized with **(C)** 20.0 wt% and **(D)** 18.0 wt% 1,4-butanediol.

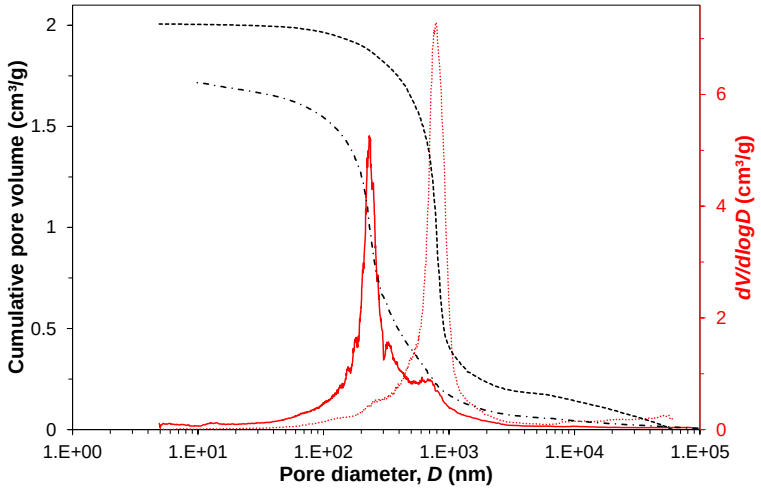

Figure S7: Mercury-intrusion porosimetry data for bulk samples of poly(BMA-*co*-EDMA-*co*-AMPS) monoliths synthesized with 20.0 wt% and 18.0 wt% 1,4-butanediol. The cumulative pore volume D_0 and pore size distribution D_3 are plotted as a function of pore diameter on a log scale. D_0 18.0 wt% 1,4-butanediol dashed line, D_0 20.0 wt% dash-dotted line, D_3 18.0 wt% dotted line, D_3 20.0 wt% solid line.

Argon adsorption-desorption experiments were also performed on both acrylates and are shown in Fig. S8 for the material synthesized with 18.0 wt% of 1,4-butanediol. These materials also feature the distinctive hysteresis between adsorption and desorption over a broad range of relative pressures, similar to what was observed with the styrene-based materials, indicating that swelling with argon is also taking place in this material.

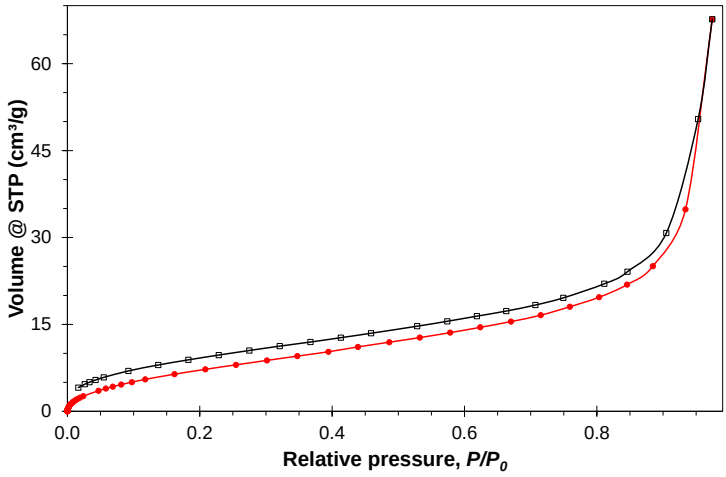

Figure S8: Argon adsorption (○) and desorption isotherms (□) for a poly(BMA-*co*-EDMA-*co*-AMPS) monolith synthesized with 18 wt% 1,4-butanediol.

When comparing the resulting pore-size distributions (Fig. S9) obtained after NLDFT treatment, again, a larger cumulative pore volume is noted for the monolith with small feature size, as could be expected based on the MIP observations. BET analysis also shows a factor 2.3 higher surface area for the acrylate with smaller feature sizes, corroborating the smaller difference in cumulative pore volume (factor 3) between the two acrylates, which is in agreement with the smaller difference in domain size (see SEMs). Both acrylates feature a distinctive trimodal PSD, as was noted for the styrene with a small feature size. Both acrylates feature globule sizes closer to the one of the styrene with small feature sizes and this trimodal character seems to be more outspoken for these small domain sizes. This seems to confirm our statement that some of the larger 15 and 25 nm pores are likely to be formed during clustering or agglomeration of the small microglobules during the formation of the polymer monoliths.

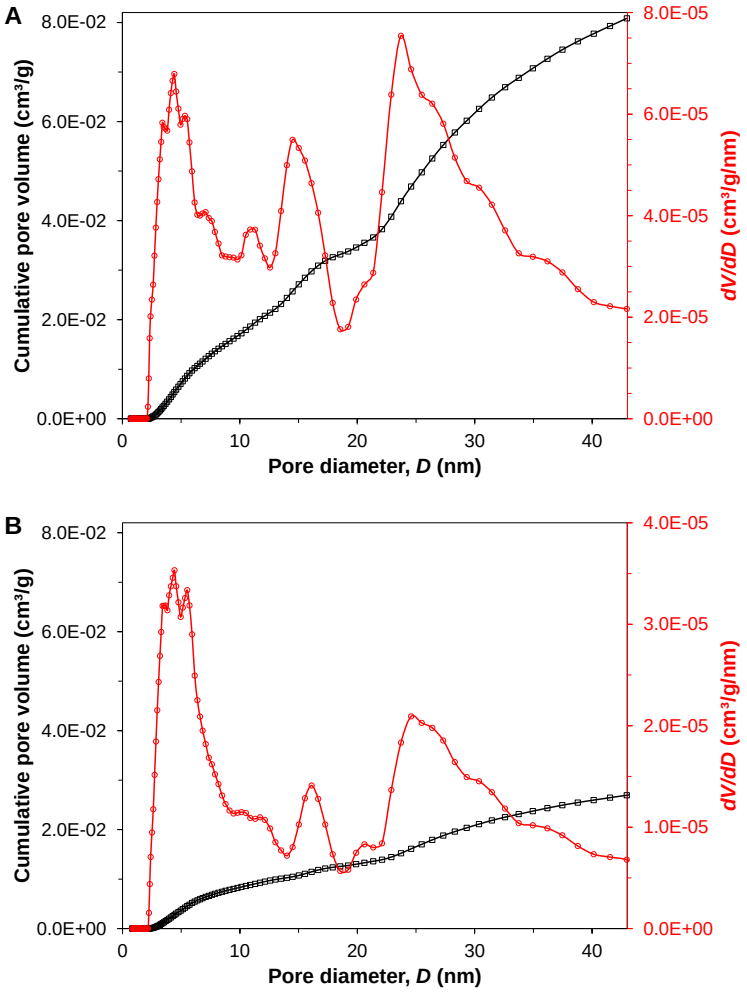

Figure S9. NLDFT-analysis results of argon-adsorption measurements on bulk samples of P(BMA-*co*-EDMA-*co*-AMPS). Pore diameter is plotted on a linear scale as a function of the cumulative pore volume D_0 (□) and pore size distribution D_2 (○) for monoliths synthesized with **(A)** 20.0 wt% and **(B)** 18.0 wt% 1,4-butanediol.